Pramana – J. Phys. (2019) 93:30
https://doi.org/10.1007/s12043-019-1793-4

Alcohol sensor based on gold-coated nanoporous anodic alumina membrane

SALEEM SHAIK[1],*, ANJANI KUMAR TIWARI[2] and S ANANTHA RAMAKRISHNA[2]

[1]Department of Materials Science and Engineering, Indian Institute of Technology Kanpur, Kanpur 208 016, India
[2]Department of Physics, Indian Institute of Technology Kanpur, Kanpur 208 016, India
*Corresponding author. E-mail: saleemsk@iitk.ac.in

MS received 5 October 2018; revised 16 January 2019; accepted 4 February 2019; published online 30 May 2019

Abstract. We report a refractive index sensor consisting of a gold-coated nanoporous anodic alumina membrane on aluminium substrate that can distinguish between different kinds of alcohols such as methanol and ethanol due to their different refractive indices. The nanoporous volume allows the loading of liquids with low surface energy into its nanopores. Upon dipping one end of the membrane into the alcohol, the entire nanoporous surface experiences wetting. The wavelength shift of the Fabry–Perot resonating modes formed between the gold-coated nanoporous alumina surface and aluminium on the other side due to the changed effective refractive index form the basis of the sensor. The sensitivity of the nanosensor to the refractive index of the loaded liquid is sufficient to distinguish between different alcohols such as methanol, ethanol and isopropanol, and to detect about 5–10% of methanol in a methanol–ethanol mixture.

Keywords. Nanoporous; wetting; Fabry–Perot resonances; sensor.

PACS Nos 78.67.Rb; 68.08.Bc; 42.60.Da; 07.07.Df

1. Introduction

Sensors are those devices that react to surroundings by sending signals according to the need of the user. If at least one dimension of the sensor size scale is smaller than about a hundred nanometre, then it can be categorised as a nanosensor. Such sensors are known for their reduced size, large surface area and excellent chemical compatibility [1] and are used to detect gases, chemicals, explosive elements and various biomolecules [2]. Nanostructures such as nanodots, nanowires, nanobelts, nanorings, nanoclusters, etc. have been promising materials for sensor applications [1–4]. Organic nanocomposite-based sensors for the detection of aldehydes in food beverages and *Escherichia coli* in water have been reported [5,6]. Surface plasmon resonance-based fibre optic sensors for the detection of human blood group, the water content in ethanol and proteins have also been reported [7–9]. A fibre-based reflectometer sensor was utilised to measure the refractive index of the transparent solid and liquid media [10]. Nanosculptured thin films with varying porosity have been used to detect vitellogenin biomarker based on surface-enhanced Raman scattering [11]. Resonance modes of terahertz metamaterials have been utilised for biosensing and temperature sensing [12]. Nanoporous structures such as zeolites, mesoporous silica and porous carbon are of special importance due to their large surface area with the possibility of versatile surface functionalisations [13–15]. Nanoporous anodic alumina (NAA) is known for their good mechanical strength, chemical properties and thermal stability [16–22]. In the recent past, NAA membranes have also been explored for sensing various biomaterials such as proteins, bacteria, viruses, cholesterol, DNA and blood serum [16,18–20].

NAA consists of long parallel nanopores in alumina that are arranged in a hexagonal lattice and can be highly optically transparent. A slab of an NAA supports Fabry–Perot (FP) modes [21,23] and waveguide modes that have used by us recently to demonstrate lasing in these systems embedded with laser dyes [24]. The n_{eff} of the NAA is determined by the pore size, inter-pore separation and medium embedded within the pores. The n_{eff} is commonly described by the Maxwell–Garnet theory (MGT) [21], or Bruggemann homogenisation

theory [17]. Highly ordered NAA are prepared usually by double anodisation of aluminium surfaces in acid environment [13]. Membranes with different pore diameters can be prepared by using different electrolytes such as sulphuric acid, oxalic acid and phosphoric acid at different anodisation voltages of 10–30, 30–70 and 40–235 V, respectively [25–28]. The nanoporous surface of the NAA enable a liquid to easily wet and spread on the surface with the liquid entering well into the nanopores [29]. The loaded liquid changes the n_{eff} of the NAA which suggests a method to detect the liquid.

In this work, we demonstrate the use of such NAA membranes to sense the presence of various alcohols and to differentiate between them using the shift in the wavelength of the FP resonances of the NAA slab due to the changed n_{eff}. The alcohol sensor made of gold-coated NAA membrane is lightweight, inexpensive and has a fast response. The gold coating is kept thin enough so as to not block the opening of the nanopores while being sufficiently thick to enhance the cavity resonance. In fact, it is known that only two kinds of alcohols are involved and it is possible to estimate their relative fractions in a mixture by measuring the refractive index. In particular, we have used this sensor to detect the presence of methanol in a mixture of methanol and ethanol. This paper is organised as follows: §2 describes the details of sample fabrication and the size distribution of the NAA nanopores. In §3, we discuss the liquid flow dynamics on the NAA surface and the identification of methanol, ethanol and its mixture by monitoring the shift of FP cavity modes. Finally, the measurements and results are summarised in §4.

2. Sample preparation

The nanoporous alumina membranes are fabricated from 250 μm thick aluminium foils (99.999% pure), cut into 1.5 cm × 2.5 cm pieces. The pieces were cleaned by ultrasonication in acetone, isopropanol, deionised (DI) water and dried with nitrogen gas. The samples were then electropolished in a mixture of perchloric acid and ethanol (volume ratio 1:4) and thoroughly rinsed in DI water to get a mirror-like finished surface. Only about 1 cm^2 electropolished area was exposed to the electrolyte with the remaining part of the sample masked with commercial lacquer. The anodisation of the sample was carried out in an electrolytic cell filled with 0.3 M oxalic acid. In the electrolytic cell, the sample surface serves as a working electrode whereas a Pt mesh is used as a counterelectrode. A stable DC power supply (Aplab, 80 V/25 Amp, VSP8025) was used to create a potential difference of 40–60 V between these electrodes. A standard two-step anodisation procedure is used to prepare the NAA samples [13]. The first anodisation is carried out for a fixed duration of 3 h. After that, the NAA was etched in the mixture of 0.4 M chromic acid and 0.2 M phosphoric acid resulting in a hexagonal textured surface, which serves as a nucleation site for the pores in the second anodisation resulting in a uniform hexagonal porous structure. The pore diameter and pore length of the NAA can be controlled by using different applied voltages or different electrolytes and by varying the second anodisation time. Figure 1a shows the field emission scanning electron microscope (FESEM) image of the NAA after second anodisation of aluminium. The nanopores are partially ordered in hexagonal fashion. Alumina pore widening was done by using wet etching in 5 wt% phosphoric acid [30,31]. The FESEM image of the etched sample is shown in figure 1b. After etching, the pore diameter increases, while the interpore distance remains constant. We deposited a 20 nm thin gold layer on the top surface of the NAA layer to increase the overall reflectivity of the NAA surface. As depicted in figure 1c, the gold deposition is non-uniform and clusters are formed on the edge of the nanopores. Importantly, the thin gold coating does not close the NAA pores entirely. Figure 1d shows the

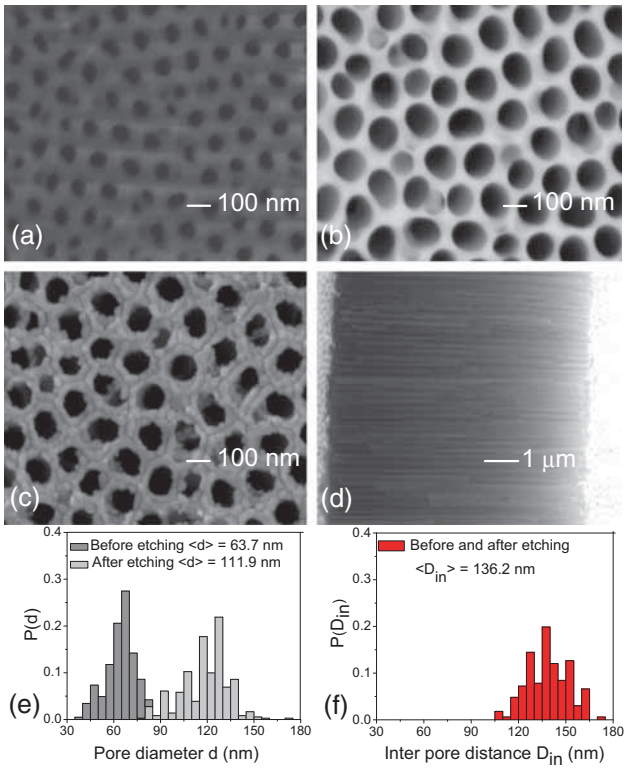

Figure 1. FESEM images of the NAA sample: (**a**) before etching, (**b**) after etching in phosphoric acid, (**c**) the gold–coated surface of the etched sample, (**d**) cross-sectional view of the gold-coated NAA, (**e**) distribution of pore diameters before and after etching and (**f**) distribution of interpore distance before and after etching.

cross-sectional view of the NAA slab. The nanopores are 5.8 μm long and straight.

To estimate the average diameter of nanopores, we analysed the size distribution utilising the FESEM image of the sample. The probability distributions of pore diameters measured over 200 nanopores of unetched and etched alumina samples are shown in figure 1e. On an average, for the unetched alumina sample, the pore diameter is about 63 nm, and for the etched sample, it is 111 nm with the standard deviation (SD) values of 9 and 11 nm. The average spacing between the pore is about 136 nm whose probability distributions are shown in figure 1f where the SD value is 13.5 nm. Before etching, the filling fraction of the porous void is around 20%. After etching with phosphoric acid, the diameter of nanopores increases to about 111 nm while the interpore spacing remains unchanged. Overall, the filling fraction of the porous void increases to about 61%.

3. Wetting behaviour of NAA surface for methanol, ethanol and isopropanol

To study the wetting dynamics of alcohols on the NAA–air interface, we gently placed a drop of 5 μl volume on the flat horizontal surface of NAA. The flow of liquid was monitored by using a CCD camera attached to a microscope at 5× magnification. The motion of the liquid front was studied by acquiring images at 25 frames per seconds. Due to wetting, the microdroplet immediately starts to spread on the NAA surface. Figures 2a, 2c and 2e show the image of the liquid front for methanol, ethanol and isopropanol, respectively, at a fixed arbitrarily starting instant ($t = 0$ s). The right panel of figures 2b, 2d and 2f depicts the liquid front after 125 frames ($t = 5$ s). Clearly, methanol spreads faster than ethanol and isopropanol. Overall, the respective flow rate of methanol, ethanol and isopropanol is about 0.7, 0.3 and 0.1 mm/s. This observable difference in liquid flow may arise due to the variation in surface tension of these alcohols which is larger for isopropanol and smaller for methanol [32]. Thus, we find that the alcohols quickly and uniformly spread on the NAA surface by filling the nanopores in the process.

4. Results and discussion

The reflection spectrum of the NAA membrane was collected by a fibre connected to a spectrometer (Ocean Optics, HR4000+, resolution ∼0.5 nm). The dark yellow curve in figure 3a shows the experimental reflection spectrum from the etched NAA sample. The reflection spectrum shows a series of peaks with frequency

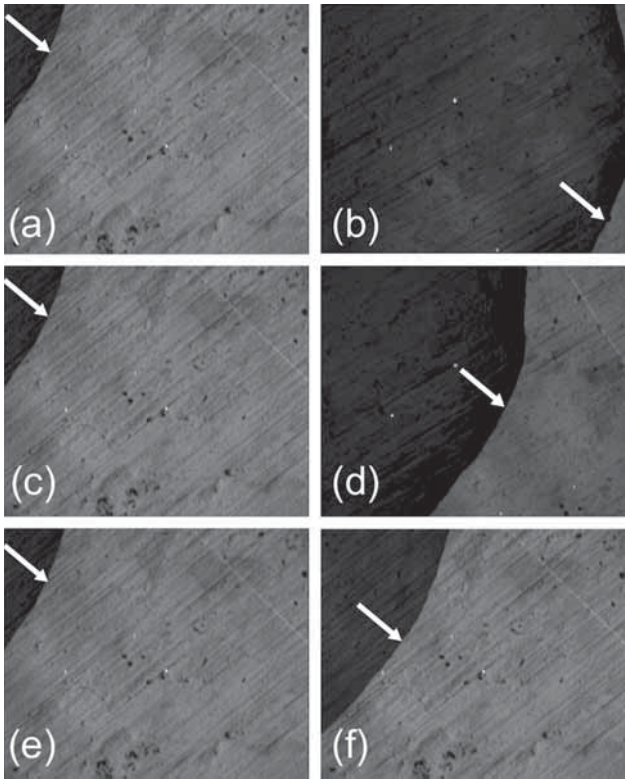

Figure 2. Images of the liquid front propagation on the gold-coated NAA for methanol, ethanol and isopropanol microdroplets. The arrows in (**a**), (**c**) and (**e**) mark the liquid fronts at $t = 0$ s and the arrows in (**b**), (**d**) and (**f**) mark the liquid fronts at $t = 5$ s.

which arises due to FP resonances and are determined principally by the thickness and effective refractive index of the NAA slab. Due to the lower reflectivity of the interfaces and light inside the sample, the modulation due to the FP resonances is weak. Nonetheless, there are 15 FP peaks between 415 and 700 nm. Around 550 nm, the free spectral range of the mode is about 18.22 nm.

The red curve in figure 3a shows the theoretically fitted reflection spectrum on the uncoated membrane. The effective refractive index of the fit parameters ($n_{\text{eff}} = \sqrt{\epsilon_{\text{eff}}\mu_{\text{eff}}}$) and the thickness ($t$) of the membrane are estimated from the FESEM image of the film. Here, $n_{\text{eff}} = \sqrt{\epsilon_{\text{eff}}\mu_{\text{eff}}}$ is calculated by the following Maxwell–Garnet formula. The theoretical fit was done by using the transfer matrix method (TMM) [33] by plugging the thickness measured from the FESEM (figure 1d). The n_{eff} value calculated from figure 1a using the Maxwell–Garnet theory depends on the pore diameter and interpore distance of the etched NAA through filling fraction (f). The expression for effective dielectric constant ϵ_{eff} of alumina is as follows:

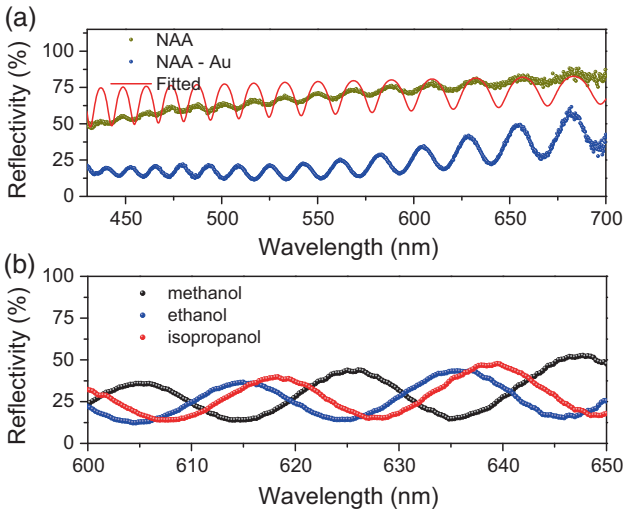

Figure 3. (**a**) Optical reflection spectrum of the NAA slab. Dark yellow curve: bare NAA slab, blue curve: NAA slab having a thin gold coating, and red curve: theoretical fit using TMM method and (**b**) reflectivity from gold-coated NAA membrane loaded with methanol (black curve), ethanol (blue curve) and isopropanol (red curve).

$$\epsilon_{\text{eff}} = \frac{\epsilon_{\text{host}}\epsilon_{\text{guest}}(1-f) + \epsilon_{\text{host}}^2(1+f)}{\epsilon_{\text{host}}(1-f) + \epsilon_{\text{guest}}(1+f)}. \quad (1)$$

Here f is the fill fraction, $f = (2\pi/\sqrt{3})(r/D_{\text{in}})^2$ where r is the radius of the nanopore, D_{in} is the inter-pore distance, $\epsilon_{\text{guest}} = \epsilon_{\text{air}} = 1$ and $\epsilon_{\text{bulk}} = \epsilon_{\text{host}} = 3.1$ are the dielectric constants of guest (air) and host (bulk alumina). The calculated n_{eff} value (=1.3) was plugged in the TMM to calculate the reflectivity of the NAA membrane. The theoretical curve shows an excellent agreement with the experimental data for a best-fit thickness parameter of 5.8 μm. When the wavelength becomes smaller, there is an increased scattering of light by the nanopores and its description as an effective medium becomes poorer. The surface interface roughness also contributes to the scattering. This diffuse scattering to a first approximation can be treated as a loss and modelled by a frequency-dependent imaginary part of the effective refractive index. As our purpose in this work was principally to demonstrate their potential as a sensor, we have simply chosen to work at red wavelengths where the effects of scattering are minimal. Hence, we have not modelled the scattering losses at smaller (blue) frequencies. The reflection spectrum of the gold-deposited NAA film is shown by the blue curve in figure 3a. Due to thin gold coating, the free spectral range does not change significantly. Nevertheless, the modulation in the reflection signal gets sharper because of increased reflectivity.

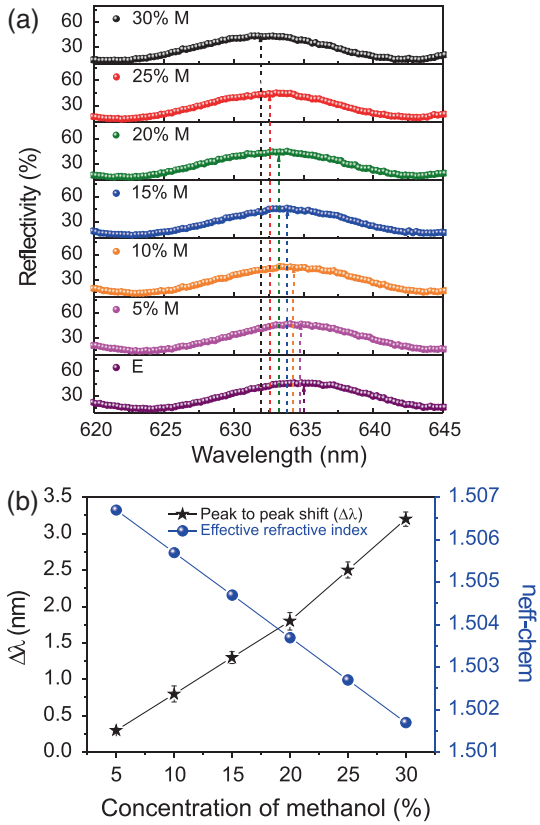

Figure 4. (**a**) Shifts in the peak reflectivity of the FP resonances for methanol–ethanol mixture with differing methanol content. The concentration of methanol is increased in steps of 5% and (**b**) variation in the effective refractive index of the mixture and FP mode shift with respect to the concentration of methanol in ethanol.

To detect various types of alcohol using reflectivity from the NAA membrane, we first filled the liquid solution in a Petri dish. After that, one end of the NAA sample was dipped (about 1 mm) into the alcohol. Due to the wetting action, the liquid quickly wets the NAA surface and moves up vertically (about 6 mm). Figure 3b shows the FP spectrum of the NAA sample when it was dipped in methanol (black curve), ethanol (blue curve) and isopropanol (red curve). The FP modulation is the characteristic of the effective refractive index of the NAA sample, and as the n_{eff} value increases, the modulation gets redshifted. As marked by the arrow in figure 3b, one of the modulation maxima for methanol appears at 625.8 nm and for ethanol and isopropanol the peak position gets shifted at 635.6 and 639.2 nm, respectively.

We used this information to further detect the amount of methanol mixed in the ethanol solvent. We essentially have a reflection reference of bare alumina and with pure ethanol. The source and the porous alumina sample are fixed so that the thickness variation of alumina does not matter. Each time the ethanol is completely

Table 1. The chemical composition and the corresponding shift.

NAA average $d = 111.9$ nm and $D_{in} = 136.2$ nm		
Chemical composition (%)	$n_{\text{eff-chem}}$	$\Delta\lambda$ (nm) with respect to ethanol
Methanol	1.487	9.8
30% methanol+70% ethanol	1.501	3.2
25% methanol+75% ethanol	1.502	2.5
20% methanol+80% ethanol	1.503	1.8
15% methanol+85% ethanol	1.504	1.3
10% methanol+90% ethanol	1.505	0.8
5% methanol+95% ethanol	1.506	0.3
Ethanol	1.507	0
Isopropanol	1.520	3.5

evaporated to get back the initial conditions. The red curve in figure 4a shows one of the FP peaks of pure ethanol. The peak is centred at 635.6 nm. When we add methanol in steps of 5 wt% in ethanol, the FP peak blue shifts due to a decrement in n_{eff}. This shift increases monotonically as the concentration of methanol increases. The shift acts as a tag to identify the amount of methanol mixed in the ethanol solvent.

The black and the blue curves in figure 3b show the respective variation of the shift ($\Delta\lambda$) in the FP mode and the effective refractive index of the mixture with respect to the percentage of methanol mixed in ethanol. The refractive index of the mixture decreases approximately by 0.001, each time we add 5% methanol. On an average, we observed a shift of 0.3 nm in wavelength for the refractive index difference of 0.001. The list of chemical compositions along with $\Delta\lambda$ and $n_{\text{eff-chem}}$ are tabulated in table 1.

Both ethanol and methanol have C–OH groups and have similar properties. In methanol, hydrogen bonds dominate over the dipole–dipole interactions and in ethanol, dipole–dipole interactions dominate over the hydrogen bonding [34]. With the addition of methanol to ethanol, the density of hydrogen bonding increases and the dipolar association of ethanol molecule decreases thereby increasing intermolecular interactions [24]. At lower (0–10%) concentrations of methanol in ethanol, the refractive index values decrease [35]. In the intermediate concentration range (10–30%), the behaviour of the refractive index becomes complicated due to various phenomena such as molecular associations, volume contraction, charge transfer, dipole-induced dipole interactions, etc. [34,35]. At higher concentrations, equilibrium state is reached, where there are no significant deviations from the effective medium properties of the mixtures.

We note that the sensitivity of this sensor is not sufficient to detect methanol (<1%) that cause contamination of alcoholic drinks. However, the proposed sensor here is principally useful in monitoring the proportions of known constituents in mixtures. We highlight below some possible uses of this sensor in chemical industry. Ethanol is actively promoted as a biofuel, but isopropanol or methanol of up to 5–10% is mixed in it to prevent its use for other purposes [36]. Methanol is a good solvent and widely used to dissolve and extract lipids such as cholesterol in the biochemical industry. Typically, a mixture of methanol (2–30%) in chloroform or ether is used [37], where again the proposed sensor could be useful to monitor the mixture. Methanol is used in pharmaceutical industry as a solvent, e.g. to extract even antibodies such as streptomycin [38]. Due to concerns of degradation in methanol, mixing ethanol has been suggested [39]. Once again, the proposed sensor would be useful to monitor such mixtures.

5. Conclusion

In conclusion, we have demonstrated a refractive index sensor based on NAA membranes and shown that it can measure the change in refractive index of an embedded liquid. This is a unique sensor which easily entraps liquids into the nanopores and allows for the presence to be measured optically through the refractive index. The wetting nature of the nanostructured surface is critically important here to load the liquid to be sensed. The presence of the liquid changes the effective refractive index of the nanoporous medium, allowing for the quantisation of the refractive index of the embedded liquid. The Maxwell–Garnet homogenisation theory is used to estimate the effective medium's refractive index. This change of the effective medium refractive index is measured by detecting the wavelength shift of the FP modes of the slab of nanoporous alumina. When the NAA membrane is coated with a thin gold layer, the modulation in the FP signal increases, thereby further increasing the sensitivity of the device. The shift in the FP modes is used to detect liquids with small refractive index differences such as methanol, ethanol, isopropanol and methanol–ethanol mixtures. By using this nanosensor, we were able to detect up to 5% methanol mixed with ethanol. The proposed nanosensor is lightweight, less expensive and has a quick response for detecting the purity level of alcohols. This NAA membrane can also be used to study intermolecular interactions of the binary mixtures of liquids, e.g. a methanol–ethanol mixture or similar mixtures.

Acknowledgements

The authors acknowledge the financial support through Project No. DST/PHY/20130147 from the Department of Science and Technology, India. Anjani Kumar Tiwari also thanks DST for the INSPIRE faculty Award (DST/INSPIRE/04/2016/002068).

References

[1] M K Patra, K Manzoor, M Manoth, S C Negi, S R Vadera and N Kumar, *Defence Sci. J.* **58**, 636 (2008)
[2] R Bogue, *Sensor Rev.* **29(4)**, 310 (2009)
[3] T-Ch Lim and S Ramakrishna, *Z. Naturforsch. A: Phys. Sci.* **61**, 402 (2006)
[4] A Vaseashta and D Dimova Malinovska, *Sci. Technol. Adv. Mater.* **6**, 312 (2005)
[5] A N Mallya, P Sowmya and P C Ramamurthy, *IEEE 2nd International Conference on Emerging Electronics* 15290572 (Indian Institute of Science, Bengaluru, 2014) p. 1
[6] A N Mallya and P C Ramamurthy, *Sensing technology: Current status and future trends III* (Springer, Wellington, New Zealand, 2015) p. 299
[7] A K Sharma, R Jha, H S Pattanaik and G J Mohr, *J. Biomed. Opt.* **14**, 064041 (2009)
[8] S K Srivastava, R Verma and B D Gupta, *Sens. Actuators B* **153**, 194 (2011)
[9] R Verma, S K Srivastava and B D Gupta, *IEEE Sens. J.* **12**, 3460 (2012)
[10] P Nath and M Buragohain, *Pramana – J. Phys.* **79**, 1525 (2012)
[11] S K Srivastava, A Shalabney, I Khalaila, C Grüner, B Rauschenbach and I Abdulhalim, *Opt. Sens.* **SeM3C-3**, 3 (2014)
[12] M Islam, S J M Rao, G Kumar, B P Pal and D R Chowdhury *Sci. Rep.* **7**, 7355 (2017)
[13] H Masuda and K Fakuda, *Science* **268(5216)**, 1466 (1995)
[14] P Xu, X Li, H Yu and T Xu, *Sensors* **14**, 19023 (2014)
[15] S Polarz and B Smarsly, *J. Nanosci. Nanotechnol.* **2(6)**, 581 (2002)
[16] A Santos, T Kumeria and D Losic, *Trends Anal. Chem.* **44**, 25 (2013)
[17] L P H-Eguía, J F-Borrull, G Macias, J Pallarès and L F Marsal, *Nanoscale Res. Lett.* **9(416)**, 1 (2014)
[18] G Sriram, P Patil, M P Bhat, R M Hegde, K V Ajeya, I Udachyan, M B Bhavya, M G Gatti, U T Uthappa, G M Neelgund, H-Y Jung, T Altalhi and M D Kurkuri, *J. Nanomater.* **2016**, 1 (2016)
[19] A Kassu, C Farley, A Sharma, W Kim and J Guo, *Sensors* **15(12)**, 29924 (2015)
[20] T Kumeria and D Losic, *Nanoscale Res. Lett.* **7(88)**, 1 (2012)
[21] A Hierro-Rodriguez, P Rocha-Rodrigues, F Valdés-Bango, J M Alameda, P A S Jorge, J L Santos, J P Araujo, J M Teixeira and A Guerreiro, *J. Phys. D* **48**, 455105 (2015)
[22] D Pratap, P Mandal and S Anantha Ramakrishna, *Pramana – J. Phys.* **83**, 1025 (2014)
[23] A Santos, V S Balderrama, M Alba, P Formentn, J Ferr-Borrull, J Pallarès and L F Marsal, *Nanoscale Res. Lett.* **7(370)**, 1 (2012)
[24] A K Tiwari, S Shaik and S A Ramakrishna, *Appl. Phys. B* **124(7)**, 127 (2018)
[25] L Zaraska, G D Sulka and M Jaskula, *J. Solid State Electrochem.* **15**, 2427 (2011)
[26] S Z Chu, K Wada, S Inoue and M Isogai, Y Katsuta and A Yasumorib, *J. Electrochem. Soc. B* **153(9)**, 384 (2006)
[27] A Belwalkar, E Grasing, W V Geertruyden, Z Huang and W Z Misiolek, *J. Memb. Sci.* **319(1-2)**, 192 (2008)
[28] R Kotha, D Strickland and A A Ayon, *Open Journal of Inorganic Nonmetallic Materials* **5**, 41 (2015)
[29] V Raspal, K O Awitor, C Massard, E Feschet-Chassot, R S P Bokalawela and M B Johnson, *Langmuir* **28(30)**, 11064 (2012)
[30] C Y Han, G A Willing, Z Xiao and H H Wang, *Langmuir* **23(3)**, 1564 (2007)
[31] J Zhang, J E Kielbasa and D L Carroll, *Mater. Chem. Phys.* **122**, 295 (2010)
[32] C Bradtmöller, A Janzen, M Crine, D Toye, E Kenig and S Scholl, *Ind. Eng. Chem. Res.* **54(10)**, 2803 (2015)
[33] J Peatross, *Physics of light and optics* (Brigham Young University Press, Utah, 2015)
[34] K Nilavarasi, T R Kartha and V Madhurima, *Spectrochim. Acta A: Mol. Biomol. Spectrosc.* **188**, 301 (2018)
[35] H Yilmaz, *Turkish J. Phys.* **26(3)**, 243 (2002)
[36] T Log and A L Moi, *Int. J. Environ. Res. Publ. Health* **15**, 2379 (2018)
[37] D B Zilversmit, *J. Lipid Res.* **5**, 300 (1964)
[38] T J Woodthorpe and D M Ireland, *J. Gen. Microbiol.* **1**, 344 (1947)
[39] H E Carter, R K Clark Jr, S R Dickman, Y H, Loo, P S Skell and W A Strong, *J. Biol. Chem.* **160**, 337 (1945)